



NIH Public Access

Author Manuscript

Biochemistry. Author manuscript; available in PMC 2014 November 12.

Published in final edited form as:

Biochemistry. 2013 November 12; 52(45): . doi:10.1021/bi400926k.

Comparison of membrane insertion pathways of the apoptotic regulator Bcl-xL and the diphtheria toxin T-domain

Mauricio Vargas-Uribe, Mykola V. Rodnin, and Alexey S. Ladokhin*

Department of Biochemistry and Molecular Biology, University of Kansas Medical Center, Kansas City, KS 66160

Abstract

The diphtheria toxin T-domain and the apoptotic repressor Bcl-xL are membrane proteins that adopt their final topology by switching folds from a water-soluble to a membrane-inserted state. While the exact molecular mechanisms of this transition are not clearly understood in either case, the similarity in the structures of soluble states of T-domain and Bcl-xL led to the suggestion that their membrane-insertion pathways will be similar as well. Previously we have applied an array of spectroscopic methods to characterize the pH-triggered refolding and membrane insertion of the diphtheria toxin T-domain. Here, we use the same set of methods to describe the membrane insertion pathway of Bcl-xL, which allows us to make a direct comparison between both systems with respect to thermodynamic stability in solution, pH-dependent membrane association and transmembrane insertion. Thermal denaturation measured by CD indicates that, unlike the T-domain, Bcl-xL does not undergo a pH-dependent destabilization of the structure. FRET measurements demonstrate that Bcl-xL undergoes reversible membrane association modulated by the presence of anionic lipids, suggesting that formation of the membrane-competent form occurs close to membrane interface. Membrane insertion of the main hydrophobic helical hairpin of Bcl-xL, α 5– α 6, was studied by site-selective attachment of environment-sensitive dye NBD. In contrast to the insertion of the corresponding TH8–TH9 hairpin in T-domain, insertion of α 5– α 6 was found not to depend strongly on the presence of anionic lipids. Taken together our results indicate that while Bcl-xL and the T-domain share structural similarities, their mode of conformational switching and membrane insertion pathways are distinctly different.

INTRODUCTION

Several classes of membrane proteins adopt their transmembrane topology posttranslationally, where they are synthesized as water-soluble structures that later insert into the bilayer in response to a given cellular signal. Examples include some bacterial toxins (1–3) and colicins (4), which are secreted to the extracellular space; and certain annexins (5) and members of the Bcl-2 proteins (6), which are synthesized as cytosolic proteins. The unique characteristic of these proteins is their ability to move from the polar environment of the aqueous medium to the non-polar milieu of the lipid bilayer, a process that clearly involves a massive refolding of the structure. The exact molecular pathways of this refolding/insertion process are not well understood, and it is not clear if different proteins follow the same pathway or share common features. In this study, we compare the membrane insertion pathways of the diphtheria toxin T-domain and the apoptotic repressor

*To whom correspondence should be addressed: Phone: 913-588-0489 FAX: 913-588-7440 aladokhin@kumc.edu.

SUPPORTING INFORMATION AVAILABLE

There is supporting information available containing 4 figures. This material is available free of charge via the Internet at <http://pubs.acs.org>.

Bcl-xL, two membrane proteins that share structural similarities in their water-soluble state (Fig. 1).

The translocation (T) domain plays a crucial role in the action of the diphtheria toxin (1, 2). The toxin, which is composed of three domains, initiates its entry to the target cell by the attachment of the receptor-binding (R) domain to its receptor in the membrane (see scheme in Fig. 2). Upon endosomal internalization and acidification, the T-domain undergoes a series of pH-triggered conformational changes that result in its membrane insertion and the translocation of the catalytic (C) domain, which holds the toxic activity, across the bilayer. The crystal structure of the T-domain in solution at neutral pH (7) (Fig. 1A) shows two central hydrophobic helices, TH8 and TH9 (red helices), surrounded by amphipathic regions (grey helices and loops). There is no high-resolution structure available for the membrane-inserted state, but the current knowledge suggests that TH8–TH9 insert as a transmembrane hairpin into the bilayer, while the rest of the structure may adopt multiple conformations (8–12). Previously, we have established the hallmarks of the membrane insertion pathway of the T-domain and the residues responsible for pH-dependent conformational switching (13–17).

Bcl-xL is an antiapoptotic member of the Bcl-2 family of proteins whose function is inhibiting the mitochondrial outer membrane permeabilization (MOMP) to prevent the cell from going into apoptosis (6, 18). The mechanism by which Bcl-xL accomplishes its action is still under debate (19–21), although it is suggested that it involves its redistribution between a cytosolic and a membrane-associated form (22, 23). From the structural point of view, Bcl-xL shares significant similarity with the diphtheria toxin T-domain (24–26). First, the high-resolution structure of Bcl-xL in the water-soluble state (24) shows a highly helical structure (Fig. 1B), with two central hydrophobic helices, α 5 and α 6 (red helices). The remaining helices (grey helices), as in the case of the T-domain, surround the hydrophobic core. Bcl-xL, however, has an additional hydrophobic helix located at the C-terminus, TM helix, which is suggested to anchor the protein to the membrane prior to insertion (25). Second, Bcl-xL is able to insert into the bilayer in response to low pH (27–30), although it is not clear if this is a prevailing signal that triggers insertion in the cell. Third, it is suggested that Bcl-xL accomplishes its blocking action of Bax (pore-forming member of the Bcl-2 family) by inserting into the bilayer as a monomer (31). Similarly, the active form of the T-domain also is a monomer (32, 33). Finally, although the high-resolution structure of Bcl-xL in the membrane-inserted state is not available either, it has been suggested that helices α 5 and α 6 insert as transmembrane regions (25, 34), like TH8–TH9 of the T-domain, whereas other regions might reside in the membrane interface.

Given the multiple similarities between the toxin and Bcl-xL, it has been proposed that the T-domain serves as model for the understanding of the action of Bcl-xL (24, 26), and by extension of other structurally similar Bcl-2 proteins (6), on the membrane. Here, we test this hypothesis by applying the same array of spectroscopic methods used in the T-domain studies to characterize the solution refolding and membrane interactions of Bcl-xL and compare them to those of the T-domain.

MATERIALS AND METHODS

Materials

Palmitoyl-oleoyl-phosphatidylcholine (POPC), palmitoyl-oleoyl-phosphatidylglycerol (POPG) and Rhodamine-PE were purchased from Avanti Polar Lipids (Alabaster, AL). IANBD-ester and AlexaFluor488-maleimide were obtained from Invitrogen (Carlsbad, CA).

Cloning and mutagenesis

Full-length Bcl-xL (residues 1–233) was PCR-amplified from cDNA obtained from K562 human lymphoma cells and ligated into the pET28b vector using the NdeI and EcoRI cloning sites. The truncated version of Bcl-xL (residues 1–207) was generated by introducing a stop codon in the position corresponding to residue 208. For the purposes of Cys-labeling with fluorescent dyes, Cys-less mutant (C151S) was created and used as template for site-directed mutagenesis. All the constructs contained an N-terminal 6×His-tag for purification.

Expression, purification and labeling

The expression and purification of Bcl-xL was based on the previously described procedure for the pET system (35). Briefly, BL-DE23pLysE *E.coli* cells were transformed with the corresponding pET plasmid and grown to OD_{600nm} ~ 0.6, after which expression was induced by addition of 0.8M IPTG and the cells grown for an additional 16 hours at 24°C. The cells were pelleted by centrifugation, lysed by sonication and clarified by centrifugation for 30 min at 4000 rpm and 4°C. The proteins were then incubated with Ni-NTA beads, washed with washing buffer (50mM Tris-HCl, 300mM NaCl, 5mM imidazole, pH 8) and eluted with 0.5M imidazole in the same buffer. The eluted proteins were subjected to size-exclusion chromatography on a Sepharose12 1×30cm column in 50mM phosphate buffer at pH 8, and quantified by measuring their absorbance spectra in the range 200–350 nm (we used molar extinction coefficient of 41,200 M⁻¹cm⁻¹ at 280 nm). Labeling with fluorescent dyes was performed using a standard procedure for thiol-reactive derivatives (13, 36) and the unreacted dye was removed by gel filtration chromatography in the same column and buffer.

LUV preparation

Large unilamellar vesicles (LUV) containing molar mixtures POPG:POPC (3:1, 1:3 and 1:9) of 0.1 μm diameter were prepared by extrusion as previously described (37, 38). Rhodamine-labeled LUV were prepared by the addition of 2% of Rhodamine-PE to the lipid mixture.

Circular dichroism and thermal unfolding

CD measurements were performed using an upgraded Jasco-720 spectropolarimeter (Japan Spectroscopic Company, Tokyo). Normally, 100 scans were recorded between 190 and 260 nm with a 1 nm step at 25°C and 95°C using a 1 mm optical path cuvette. The sample contained 4μM of Bcl-xL in 50mM phosphate buffer at pH 8.0 or a mixture of phosphate and acetic/acetate buffer at pH 6.0, 5.0 or 4.0. Further acidification was reached by equilibrating the sample in 50mM glycine-HCl buffer. All spectra were corrected for background. The thermal unfolding was followed at 222 nm with a 1 degree/minute scan rate, unless indicated. The data was fitted to a two-state transition as described before (15, 17), obtaining the transition temperature T_m and transition enthalpy ΔH°.

Fluorescence measurements and analysis

Steady-state fluorescence emission was measured using a SPEX Fluorolog FL3-22 steady-state fluorescence spectrometer (Jobin Yvon, Edison, NJ) equipped with double-grating excitation and emission monochromators. The measurements were made in a 2°10 mm cuvette oriented perpendicular to the excitation beam and maintained at 25°C using a Peltier device from Quantum Northwest (Spokane, WA) in 1 nm steps. For Alexa488 measurements, we recorded the emission spectra from 470 to 700 nm with excitation wavelength of 455 nm and slits of 2 nm for both excitation and emission. For NBD measurements, we collected the emission spectra from 490 to 700 nm, and the excitation

wavelength was 470 nm, using slits of 5 nm on both monochromators. For each spectrum, we averaged 5 scans after incubating the samples during 30 min for equilibration.

Fluorescence decays were measured with a time-resolved fluorescence spectrometer, FluoTime 200 (PicoQuant, Berlin, Germany), using a standard time-correlated single-photon counting scheme as previously described (39). Samples were excited at 440 nm by a subnanosecond pulsed diode laser, LDH 440 (PicoQuant, Berlin, Germany), with a repetition rate of 10 MHz. Fluorescence emission was detected at 535 nm, selected by a Scicentech Model 9030 monochromator, using a PMA-182 photomultiplier (PicoQuant, Berlin, Germany). The samples normally contained 0.3 μM protein and 0.5 mM lipid. The fluorescence intensity decay was analyzed using FluoFit iterative-fitting software based on the Marquardt algorithm (PicoQuant, Berlin, Germany).

The pH-dependencies of the fraction of membrane-bound or membrane-inserted states generated by corresponding spectroscopic experiments were fitted to the following equation (40):

$$F = \frac{1}{1 + 10^{n(pH - pK)}} \quad (1)$$

where pK is a negative logarithm of the dissociation constant, and n is the Hill coefficient.

RESULTS AND DISCUSSION

On the choice of experimental models for insertion studies

The diphtheria toxin is composed of three domains: the C-domain (residues 1–199), the T-domain (residues 200–378) and the R-domain (residues 379–535). The C-domain inhibits protein synthesis in the target cell and must enter the cytosol to execute its action. The R-domain is responsible for the initial attachment of the toxin to the target cell through a direct interaction with a membrane receptor (Fig. 2A). The membrane insertion of the T-domain and translocation of the C-domain across the bilayer, however, does not take place at this point, because the T-domain requires the acidification of the medium, which occurs at a later stage inside the endosome (1). As a consequence, the T-domain retains the water-soluble structure regardless of the attachment of the entire toxin to the membrane. The isolated T-domain has been shown to be able to translocate its own terminus in model membrane systems (along with the C-domain, if attached (41)) as well as to ensure translocation of various molten globule-like proteins (42). Hence, the isolated T-domain has been a choice model for numerous biophysical studies on membrane binding and insertion (8–17, 33, 43–46).

What would be an appropriate version of Bcl-xL to be compared to the T-domain with regard to membrane insertion? The initial attachment of Bcl-xL to the mitochondrial membrane is ensured by a single TM helical fragment (residues 208–233). The folded N-terminal region (oval in Fig. 2B) remains in a water-soluble state (25) and does not enter the membrane prior to the activation, which at least in model systems can be achieved by the change in pH (27–30). This arrangement is similar to that of the diphtheria toxin, with the TM fragment and the N-terminal domain of Bcl-xL being equivalent to the R-domain and the T-domain of the toxin, respectively. Therefore, most of the presented results were generated with a Bcl-xL version in which the C-terminal TM helix has been truncated. Thus, the comparison made in this study corresponds to the membrane binding and insertion processes of the N-terminal domain of Bcl-xL (residues 1–207) and the isolated T-domain (residues 200–378), depicted as curved arrows in Fig. 2.

The truncation of the TM helix in Bcl-xL offers important additional advantages since it allows the study of the initial association of the protein with the membrane interface. The FRET assay used in this study for measuring this association was developed, and validated using independent FCS measurements, for the case of the T-domain (13). The assay uses the donor in the protein and the acceptor attached to a lipid head group, and requires that the protein and the membrane interface are not within the Förster distance of the donor/acceptor pair prior to the interaction. If the protein is already anchored to bilayer due to the TM helix, then the donor and acceptor would be within the Förster distance, and no spectral changes may be observed when triggering the binding of the N-terminal region of Bcl-xL to the membrane interface. Thus, by truncating the TM helix, we aim to prevent the N-terminal domain of Bcl-xL to be anchored to the bilayer, and hence, ensure a detectable change in the fluorescent signal upon donor/acceptor interaction. Hereafter, the truncated construct of the protein will be simply referred as Bcl-xL.

pH-dependent stability in solution

The diphtheria toxin T-domain inserts into the bilayer through pH-triggered conformational changes that occur in solution and in the membrane, going along multiple intermediate states until reaching the final transmembrane conformation (13). The first conformational change occurs in solution with a midpoint pH of 6.2 and corresponds to the conversion of the water-soluble state (W-state) into the membrane-competent state (W^+ -state) as a result of the protonation of key histidine residues (2, 14, 16). The resulting W^+ -state, while different from a molten globule state populated at $pH < 5$ (as discussed in (2)), is nevertheless characterized by partial refolding, reduction in the amount of secondary structure and loss of thermostability (14, 16, 17). To determine whether the pH-triggered membrane insertion of Bcl-xL goes through the formation of the same intermediate, we tested the pH-induced loss of secondary structure by CD spectroscopy (Fig. 3A). The CD spectrum in solution at pH 8 has the typical features of an α -helical protein (black spectrum), consistent with the high-resolution structure in solution (24), with minima of ellipticity at ~ 208 and ~ 222 nm, and a maximum at around ~ 190 nm. Upon acidification, the CD spectrum of Bcl-xL maintained its characteristic shape and exhibits marginal reduction in molar ellipticity changes (Fig. 3), indicating that Bcl-xL does not experience a pH-induced loss of secondary structure. This behavior is different from that of the T-domain (Fig. 3B), which loses substantial part of its ellipticity signal in the same pH range (44, 45).

We then tested the pH-induced loss of thermodynamic stability by measuring changes in ellipticity at 222 nm as a function of temperature. On the first step we have established that thermal unfolding of Bcl-xL is reversible and rate-independent (Supplementary Fig. S1), which are prerequisites for quantitative analysis. To provide a visual reference, we display the fits for the previously published thermal unfolding data for the T-domain (17) in Fig. 4A. These results indicate a substantial loss of stability when pH is reduced from 8 to 6, which follows from an over 15°C reduction in the melting temperature and a loss in transition enthalpy ΔH° (Thermodynamic parameters for the thermal denaturation of both proteins are summarized in Table 1). Cooperative melting transition is no longer observed at pH 5, when the T-domain is converted to the W^+ -state (Fig. 4A, blue line). In contrast, we observe identical thermal transitions of Bcl-xL at pH 8 and 6 (Fig. 4B). Moreover, further acidification up to pH 4 causes only a small decrease in melting temperature and transition enthalpy (Fig. 4B and Table 1). These results clearly indicate that the solution fold Bcl-xL is not destabilized by acid, complementing a previous report that showed Bcl-xL being equally resistant to chemical denaturation at neutral or acidic pH (47). Together, our measurements suggest that Bcl-xL does not go through a CD-detectable pH-induced conformational change in the aqueous phase as does the T-domain, demonstrating the difference at the very early stages of the membrane insertion pathways.

Membrane association

Previously we have reported pH dependence of membrane binding of the T-domain to vesicles of various lipid compositions using several independent spectroscopic methods, which produced results with excellent agreement (13, 16). One of them, based on FRET methodology, is used here for Bcl-xL. Briefly, the donor dye (Alexa488) is attached to the protein and the acceptor (Rhodamine) is incorporated in the lipid vesicle as Rhodamine-PE. When protein and vesicles are mixed together at various pH, the binding can be measured by the decrease in the emission intensity of the donor or by the shortening of its fluorescence life-time. We show representative results of the steady-state (Fig. 5A) and life-time (Fig. 5B) fluorescence measurements for membrane interaction of the Bcl-xL R102C mutant with selectively attached dye to the cysteine residue. As expected, the data indicate a decrease in the fluorescence intensity and faster fluorescence decay when the interaction between the donor and acceptor is triggered by acidification (steps 1 and 2, black and blue). These spectral changes do not occur in the absence of acceptor (Supplementary Fig. S2), and therefore are consistent with the association of labeled Bcl-xL with the membrane. Importantly, the process is reversible, since the spectral features are recovered upon return to pH 8 (step 3, red), allowing the thermodynamic treatment to the data.

For the T-domain, the initial binding proceeds through an interfacial intermediate I-state and is largely independent of the physical-chemical properties of the membrane interface (13). We tested whether this would also hold true for Bcl-xL by measuring the association of the protein to LUV of different lipid compositions as a function of the pH. To do so, we used the FRET assay described above, and we calculated the FRET efficiency of binding at different pH values. (We have also tested whether the position of labeling affected this measurement by using three different single-cysteine mutants G70C, R102C or S110C. The resulting pH-dependent binding profiles are superimposable (Supplementary Fig. S3), indicating that we can label any of the three residues with the donor dye without affecting membrane binding). In Fig. 6A, we show the titration curves previously obtained in the case of the T-domain (13), where it is evidenced that regardless of the proportion of the anionic lipid POPG in the LUV, the pK of the transition remains mostly unaltered. The case of Bcl-xL (Fig. 6B), however, appears to be different. In this case, the decrease of the POPG content causes a shift in the pK of the transition, indicating that the binding of the protein to the bilayer depends on the physical-chemical properties of the membrane interface. Furthermore, Bcl-xL was unable to bind to LUV composed of only 10% anionic lipid (cyan), indicating that POPG is critical for binding of the protein to the membrane. Thus, in contrast to the case of the T-domain, our results indicate that the formation of the membrane-competent state of Bcl-xL responds to changes in the physical-chemical environment of the membrane interface.

This difference in the binding to the membrane interface implies that both proteins respond to the pH changes at different stages of the process. In the case of the T-domain, the protein would respond to acidification when still in the bulk solution because 1) the low pH causes conformational changes in the absence of membranes (Fig. 3 and 4, and references (14, 16, 17, 44)) and 2) binding to the bilayer does not depend on the physical-chemical properties of the membrane interface (Fig. 6 and reference (13)). In the case of Bcl-xL, however, the opposite is true: 1) no changes are observed during the acidification in the absence of membranes (Fig. 3 and 4), and 2) there is a strong dependence on the content of POPG (Fig. 6). The charges on the POPG head group will create a negative surface potential that can either affect the pKa's of key titratable groups of Bcl-xL directly or possibly modulate the local pH near the interface, or both (48, 49).

Membrane insertion of the hydrophobic helical hairpin

The next step in the insertion pathway of the T-domain is an interfacial refolding and membrane insertion of the hydrophobic helical hairpin TH8–TH9 (Fig. 1A, red helices) to form a transmembrane T-state (13). The formation of this state can be followed experimentally by attaching the environment-sensitive fluorescent probe NBD to a single-cysteine mutant in the middle of helix TH9 (13, 15). A similar transition is predicted to occur for Bcl-xL, as the helices $\alpha 5-\alpha 6$ (Fig. 1B, red helices) have been observed to adopt a transmembrane topology in the context of the isolated fragments (25). To confirm that these helices can be inserted in the context of protein, we labeled helix $\alpha 6$ at position N175C (Fig. 1B) with NBD. We show a typical measurement in Fig. 7, where the acidification of the medium in the presence of LUV (steps 1 and 2, black and blue) results in a 12 nm blue-shift and 7-fold increase of the intensity in the emission spectra (Fig. 7A), and longer fluorescence decay (Fig. 7B) of the NBD-labeled Bcl-xL. These spectral changes are consistent with the repositioning of the probe to a non-polar environment, where the fact that it does not occur in the absence of the LUV (Supplementary Fig. S4) suggests that the spectral changes are the result of the probe locating within the hydrocarbon core. The return to pH 8.0 causes the recovery of the spectral features and life-time decay, which indicates that this insertion process is reversible (step 3, red).

The pH dependence of this insertion is affected by the mole fraction of POPG in the T-domain, where a high proportion of anionic lipid is required for the protein to adopt the T-state (13). In Fig. 8A, we show the fitting curves for the pH-dependence of the insertion of the T-domain as a reference. We made the parallel analysis for the hairpin of Bcl-xL by using the NBD-labeled protein as described above and measuring the changes in intensity as a function of the pH. The normalized data is presented in Fig. 8B, where it is observed that the pH dependence varied just slightly when decreasing the mole fraction of POPG in the membrane. The data for LUV composed of 10% POPG was excluded from the analysis since there were no spectral changes observed, due to the lack of association of Bcl-xL with the membrane under those conditions in the first place (see Fig. 6B). The T-domain is fully bound to the membrane under those same conditions (see Fig. 6A), and therefore, the lack of membrane insertion is due to the protein being trapped in a previous kinetic intermediate in the membrane interface. In contrast, pH-dependencies of insertion of Bcl-xL only marginally differ from those of initial association, suggesting that the non-inserted state on membrane interface exists only transiently. Thus, the insertion of the helical hairpins also takes place by a different mechanism, where the T-domain responds to the presence of anionic lipid for this step, but not Bcl-xL.

SUMMARY

We summarize our findings in Fig. 9, where we illustrate the comparison of the insertion pathways for the T-domain and Bcl-xL. The structures of the soluble W-states are similar for the two proteins (7, 24), featuring a pair of long hydrophobic helices in the middle of the structure (highlighted red in Fig. 1): TH8–TH9 and $\alpha 5-\alpha 6$ for the T-domain and Bcl-xL, respectively. While these helices will adopt a transmembrane conformation in the final inserted T-state in both cases, the similarities between the two proteins end there. For the case of the T-domain (Fig. 9A), the folded soluble W-state is initially converted to the partially unfolded membrane-competent W^+ -state as a result of acidification of solution. This W^+ -state then interacts with the membrane in a manner that is independent of the properties of the membrane interface, indicating that the initial pH-dependent conformational switching event occurs in solution (13, 16). The physiological benefit for this feature is likely to be related to the fact that the toxin may dissociate from its receptor inside the endosome (50) and the T-domain is no longer localized close to membrane interface. The pathway proceeds through a series of intermediate states, such as interfacial I-

state and activated insertion-competent I⁺-state (13). The final insertion to T-state is regulated by additional protonation on the membrane interface and by the presence of anionic lipids, presumably promoting formation of productive intermediates via electrostatic interactions with cationic groups on the T-domain.

Remarkably, the soluble W-state of Bcl-xL is not destabilized by acidification and the formation of the membrane-competent state does not appear to require a conformational change to occur in solution (Fig. 3 and 4). Unlike in the case of the T-domain, the conformational switching initiating the insertion cascade requires the membrane interface and is modulated by the presence of anionic lipids (Fig. 6). (It is possible that this difference is related to the possibility that the protonation of acidic residues plays a more prominent role in case of Bcl-xL, than in the case of the T-domain, for which histidine protonation has been established as a key factor modulating pH-dependent refolding and membrane insertion (2, 14–17). The exact molecular mechanism of lipid modulation of Bcl-xL binding to membranes and the identity of the residues involved in pH-dependent conformational switching on the lipid-water interface, however, will be a subject of future studies involving mutagenesis and various lipid compositions). Once the protein is on the interface, the insertion proceeds without the requirement of additional protonation in a lipid-independent manner, which is again different from the behavior of the T-domain (Fig. 8). Thus, our study clearly indicates that Bcl-xL and the diphtheria toxin T-domain insert into the lipid bilayer following different membrane insertion and protonation pathways. We suggest that the difference in the nature of the conformational switching in both proteins evolved to best serve their physiological function. For the T-domain, the robustness of delivery of its cargo (the catalytic domain, ultimately responsible for toxicity) requires no regulation step and is achieved by a single copy of the protein. In contrast, Bcl-xL and other proteins of the Bcl-2 family act collectively, and their function is very tightly regulated (6, 19, 20). Subsequently, lipid-dependent triggering of the insertion (Fig. 6) can be a part of such regulatory machinery. Another important aspect of membrane interactions of Bcl-xL is the complete reversibility of binding (Fig. 5) and insertion (Fig. 7), also suggested previously (28), which may be required for proper functioning of this protein.

Supplementary Material

Refer to Web version on PubMed Central for supplementary material.

Acknowledgments

We thank Dr. Kenneth Peterson for the kind donation of cDNA obtained from K562 human lymphoma cells that served as template for the cloning of Bcl-xL. We are grateful to Mr. M.A. Myers for his editorial assistance.

This research was supported by NIH grant GM-069783. M.V.U. was partially supported by Fulbright-CONICYT

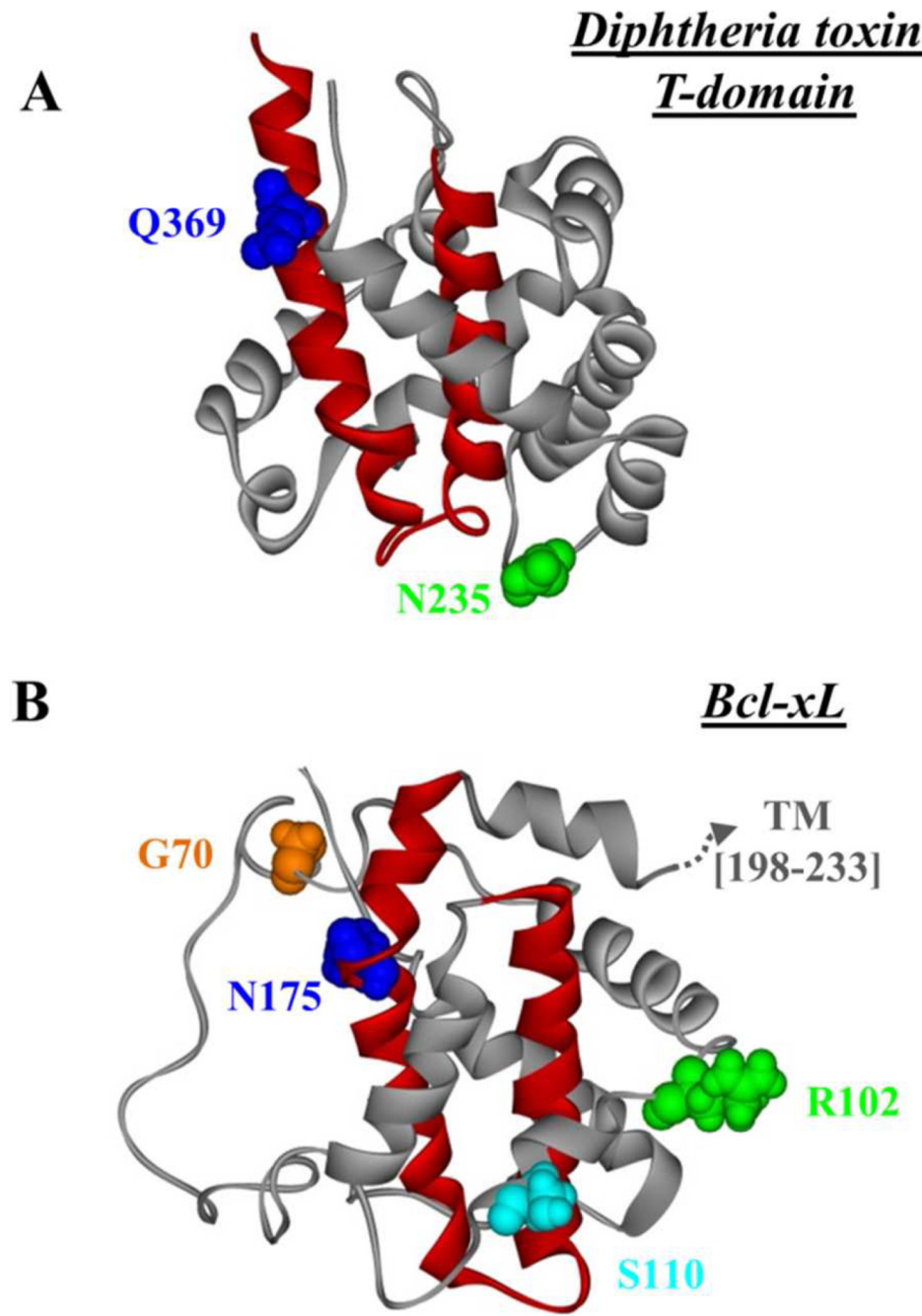
REFERENCES

1. Murphy JR. Mechanism of diphtheria toxin catalytic domain delivery to the eukaryotic cell cytosol and the cellular factors that directly participate in the process. *Toxins (Basel)*. 2011; 3:294–308. [PubMed: 22069710]
2. Ladokhin AS. pH-triggered conformational switching along the membrane insertion pathway of the diphtheria toxin T-domain. *Toxins (Basel)*. 2013; 5:1362–1380. [PubMed: 23925141]
3. Young JA, Collier RJ. Anthrax Toxin: Receptor Binding, Internalization, Pore Formation, and Translocation. *Annu Rev Biochem*. 2007; 76:243–265. [PubMed: 17335404]
4. Cramer WA, Heymann JB, Schendel SL, Deriy BN, Cohen FS, Elkins PA, Stauffacher CV. Structure-function of the channel-forming colicins. *Annu. Rev. Biophys. Biomol. Struc.* 1995; 24:611–641.

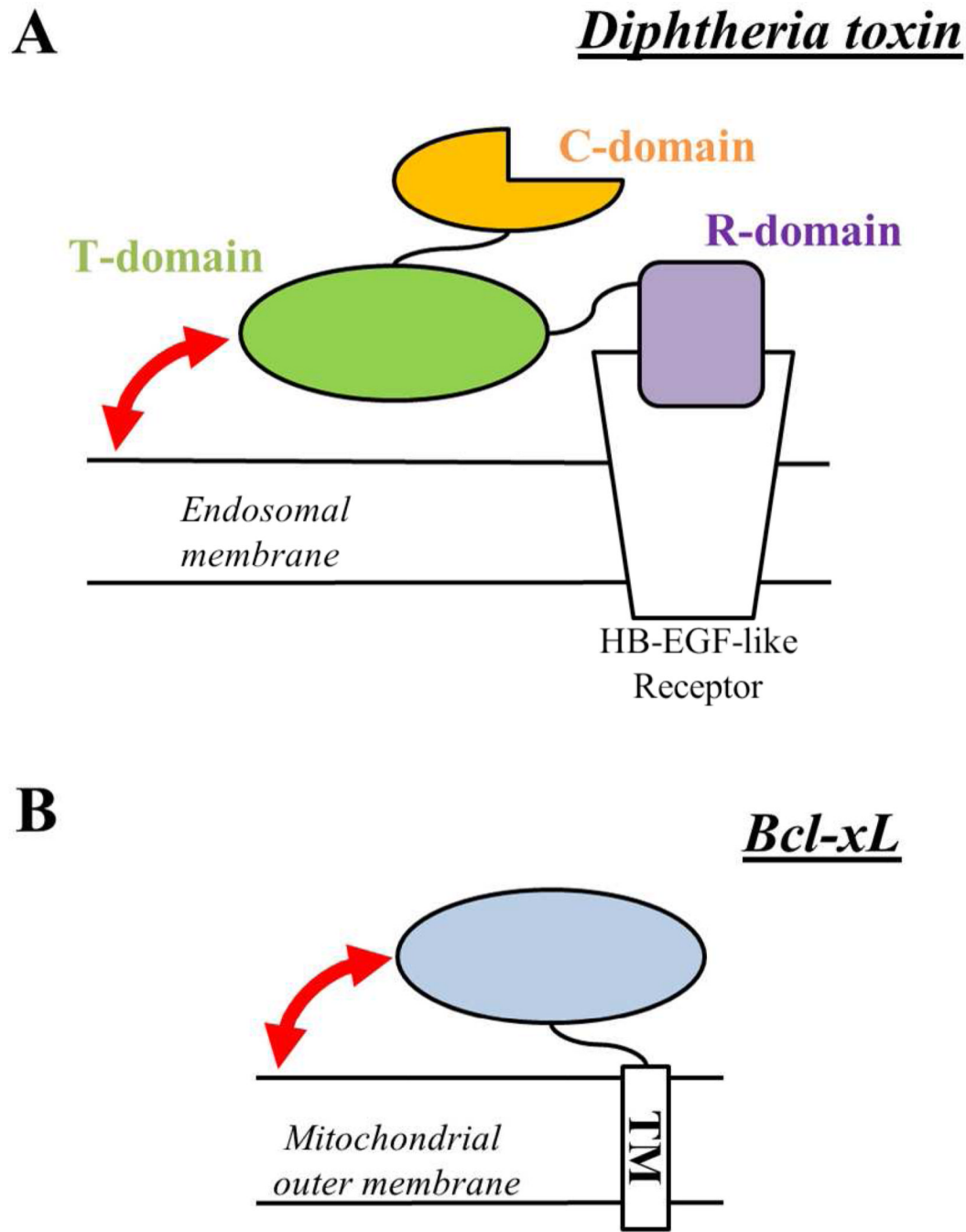
5. Gerke V, Moss SE. Annexins: From structure to function. *Physiological Reviews*. 2002; 82:331–371. [PubMed: 11917092]
6. Youle RJ, Strasser A. The BCL-2 protein family: opposing activities that mediate cell death. *Nat Rev Mol Cell Biol*. 2008; 9:47–59. [PubMed: 18097445]
7. Bennett MJ, Eisenberg D. Refined structure of monomeric diphtheria toxin at 2.3 Å resolution. *Protein Sci*. 1994; 3:1464–1475. [PubMed: 7833808]
8. Oh KJ, Zhan H, Cui C, Hideg K, Collier RJ, Hubbell WL. Organization of diphtheria toxin T domain in bilayers: A site-directed spin labeling study. *Science*. 1996; 273:810–812. [PubMed: 8670424]
9. Oh KJ, Zhan H, Cui C, Altenbach C, Hubbell WL, Collier RJ. Conformation of the diphtheria toxin T domain in membranes: A site-directed spin-labeling study of the TH8 helix and TL5 loop. *Biochemistry*. 1999; 38:10336–10343. [PubMed: 10441127]
10. Rosconi MP, Zhao G, London E. Analyzing topography of membrane-inserted diphtheria toxin T domain using BODIPY-streptavidin: At low pH, helices 8 and 9 form a transmembrane hairpin but helices 5–7 form stable nonclassical inserted segments on the cis side of the bilayer. *Biochemistry*. 2004; 43:9127–9139. [PubMed: 15248770]
11. Senzel L, Gordon M, Blaustein RO, Oh KJ, Collier RJ, Finkelstein A. Topography of diphtheria toxin's T domain in the open channel state. *J. Gen. Physiol*. 2000; 115:421–434. [PubMed: 10736310]
12. Wang Y, Malenbaum SE, Kachel K, Zhan HJ, Collier RJ, London E. Identification of shallow and deep membrane-penetrating forms of diphtheria toxin T domain that are regulated by protein concentration and bilayer width. *J. Biol. Chem*. 1997; 272:25091–25098. [PubMed: 9312118]
13. Kyrychenko A, Posokhov YO, Rodnin MV, Ladokhin AS. Kinetic intermediate reveals staggered pH-dependent transitions along the membrane insertion pathway of the diphtheria toxin T-domain. *Biochemistry*. 2009; 48:7584–7594. [PubMed: 19588969]
14. Rodnin MV, Kyrychenko A, Kienker P, Sharma O, Posokhov YO, Collier RJ, Finkelstein A, Ladokhin AS. Conformational switching of the diphtheria toxin T domain. *J Mol Biol*. 2010; 402:1–7. [PubMed: 20654627]
15. Rodnin MV, Kyrychenko A, Kienker P, Sharma O, Vargas-Uribe M, Collier RJ, Finkelstein A, Ladokhin AS. Replacement of C-terminal histidines uncouples membrane insertion and translocation in diphtheria toxin T-domain. *Biophys J*. 2011; 101:L41–L43. [PubMed: 22098755]
16. Kurnikov IV, Kyrychenko A, Flores-Canales JC, Rodnin MV, Simakov N, Vargas-Uribe M, Posokhov YO, Kurnikova M, Ladokhin AS. pH-Triggered Conformational Switching of the Diphtheria Toxin T-Domain: The Roles of N-Terminal Histidines. *J Mol Biol*. 2013; 425:2752–2764. [PubMed: 23648837]
17. Vargas-Uribe M, Rodnin MV, Kienker P, Finkelstein A, Ladokhin AS. Crucial Role of H322 in Folding of the Diphtheria Toxin T-Domain into the Open-Channel State. *Biochemistry*. 2013; 52:3457–3463. [PubMed: 23621842]
18. Wang C, Youle RJ. The role of mitochondria in apoptosis*. *Annu Rev Genet*. 2009; 43:95–118. [PubMed: 19659442]
19. Shamas-Din A, Kale J, Leber B, Andrews DW. Mechanisms of action of bcl-2 family proteins. *Cold Spring Harb Perspect Biol*. 2013; 5
20. Garcia-Saez AJ. The secrets of the Bcl-2 family. *Cell Death Differ*. 2012; 19:1733–1740. [PubMed: 22935609]
21. Soriano ME, Scorrano L. Traveling Bax and forth from mitochondria to control apoptosis. *Cell*. 2011; 145:15–17. [PubMed: 21458662]
22. Edlich F, Banerjee S, Suzuki M, Cleland MM, Arnoult D, Wang C, Neutzner A, Tjandra N, Youle RJ. Bcl-x(L) retrotranslocates Bax from the mitochondria into the cytosol. *Cell*. 2011; 145:104–116. [PubMed: 21458670]
23. Hsu YT, Wolter KG, Youle RJ. Cytosol-to-membrane redistribution of Bax and Bcl-X(L) during apoptosis. *Proc Natl Acad Sci U S A*. 1997; 94:3668–3672. [PubMed: 9108035]
24. Muchmore SW, Sattler M, Liang H, Meadows RP, Harlan JE, Yoon HS, Nettesheim D, Chang BS, Thompson CB, Wong SL, Ng SL, Fesik SW. X-ray and NMR structure of human Bcl-xL, an inhibitor of programmed cell death. *Nature*. 1996; 381:335–341. [PubMed: 8692274]

25. García-Sáez AJ, Mingarro I, Pérez-Payá E, Salgado J. Membrane-insertion fragments of Bcl-XL, Bax. *Bid. Biochemistry*. 2004; 43:10930–10943. [PubMed: 15323553]
26. Antignani A, Youle RJ. How do Bax and Bak lead to permeabilization of the outer mitochondrial membrane? *Curr Opin Cell Biol*. 2006; 18:685–689. [PubMed: 17046225]
27. Minn AJ, Velez P, Schendel SL, Liang H, Muchmore SW, Fesik SW, Fill M, Thompson CB. Bcl-x(L) forms an ion channel in synthetic lipid membranes. *Nature*. 1997; 385:353–357. [PubMed: 9002522]
28. Thuduppathy GR, Terrones O, Craig JW, Basanez G, Hill RB. The N-terminal domain of Bcl-xL reversibly binds membranes in a pH-dependent manner. *Biochemistry*. 2006; 45:14533–14542. [PubMed: 17128992]
29. Thuduppathy GR, Craig JW, Kholodenko V, Schon A, Hill RB. Evidence that membrane insertion of the cytosolic domain of Bcl-xL is governed by an electrostatic mechanism. *J Mol Biol*. 2006; 359:1045–1058. [PubMed: 16650855]
30. Garcia-Saez AJ, Ries J, Orzaez M, Perez-Paya E, Schwille P. Membrane promotes tBID interaction with BCL(XL). *Nat Struct Mol Biol*. 2009; 16:1178–1185. [PubMed: 19820711]
31. Billen LP, Kokoski CL, Lovell JF, Leber B, Andrews DW. Bcl-XL inhibits membrane permeabilization by competing with Bax. *PLoS Biol*. 2008; 6:e147. [PubMed: 18547146]
32. Gordon M, Finkelstein A. The number of subunits comprising the channel formed by the T domain of diphtheria toxin. *J Gen Physiol*. 2001; 118:471–480. [PubMed: 11696606]
33. Palchevskyy SS, Posokhov YO, Olivier B, Popot JL, Pucci B, Ladokhin AS. Chaperoning of Insertion of Membrane Proteins into Lipid Bilayers by Hemifluorinated Surfactants: Application to Diphtheria Toxin. *Biochemistry*. 2006; 45:2629–2635. [PubMed: 16489756]
34. Franzin CM, Choi J, Zhai D, Reed JC, Marassi FM. Structural studies of apoptosis and ion transport regulatory proteins in membranes. *Magn Reson Chem*. 2004; 42:172–179. [PubMed: 14745797]
35. Zhan H, Oh KJ, Shin Y-K, Hubbell WL, Collier RJ. Interaction of the isolated transmembrane domain of diphtheria toxin with membranes. *Biochemistry*. 1995; 34:4856–4863. [PubMed: 7718592]
36. Haugland, RP. Handbook of Fluorescent Probes and Research Chemicals. 6th ed.. Eugene, OR: Molecular Probes, Inc.; 1996.
37. Hope MJ, Bally MB, Mayer LD, Janoff AS, Cullis PR. Generation of multilamellar and unilamellar phospholipid vesicles. *Chem. Phys. Lipids*. 1986; 40:89–107.
38. Mayer LD, Hope MJ, Cullis PR. Vesicles of variable sizes produced by a rapid extrusion procedure. *Biochim. Biophys. Acta*. 1986; 858:161–168. [PubMed: 3707960]
39. Posokhov YO, Ladokhin AS. Lifetime fluorescence method for determining membrane topology of proteins. *Anal Biochem*. 2006; 348:87–93. [PubMed: 16298322]
40. Ladokhin AS. Fluorescence spectroscopy in thermodynamic and kinetic analysis of pH-dependent membrane protein insertion. *Methods Enzymol*. 2009; 466:19–42. [PubMed: 21609856]
41. Oh KJ, Senzel L, Collier RJ, Finkelstein A. Translocation of the catalytic domain of diphtheria toxin across planar phospholipid bilayers by its own T domain. *Proc. Natl. Acad. Sci. USA*. 1999; 96:8467–8470. [PubMed: 10411898]
42. Ren J, Kachel K, Kim H, Malenbaum SE, Collier RJ, London E. Interaction of diphtheria toxin T domain with molten globule-like proteins and its implications for translocation. *Science*. 1999; 284:955–957. [PubMed: 10320374]
43. Ladokhin AS, Legmann R, Collier RJ, White SH. Reversible refolding of the diphtheria toxin T-domain on lipid membranes. *Biochemistry*. 2004; 43:7451–7458. [PubMed: 15182188]
44. Rodnin MV, Posokhov YO, Contino-Pepin C, Brettmann J, Kyrychenko A, Palchevskyy SS, Pucci B, Ladokhin AS. Interactions of fluorinated surfactants with diphtheria toxin T-domain: testing new media for studies of membrane proteins. *Biophys J*. 2008; 94:4348–4357. [PubMed: 18310255]
45. Kyrychenko A, Rodnin MV, Vargas-Uribe M, Sharma SK, Durand G, Pucci B, Popot JL, Ladokhin AS. Folding of diphtheria toxin T-domain in the presence of amphipols and fluorinated surfactants: Toward thermodynamic measurements of membrane protein folding. *Biochim Biophys Acta*. 2012; 1818:1006–1012. [PubMed: 21945883]

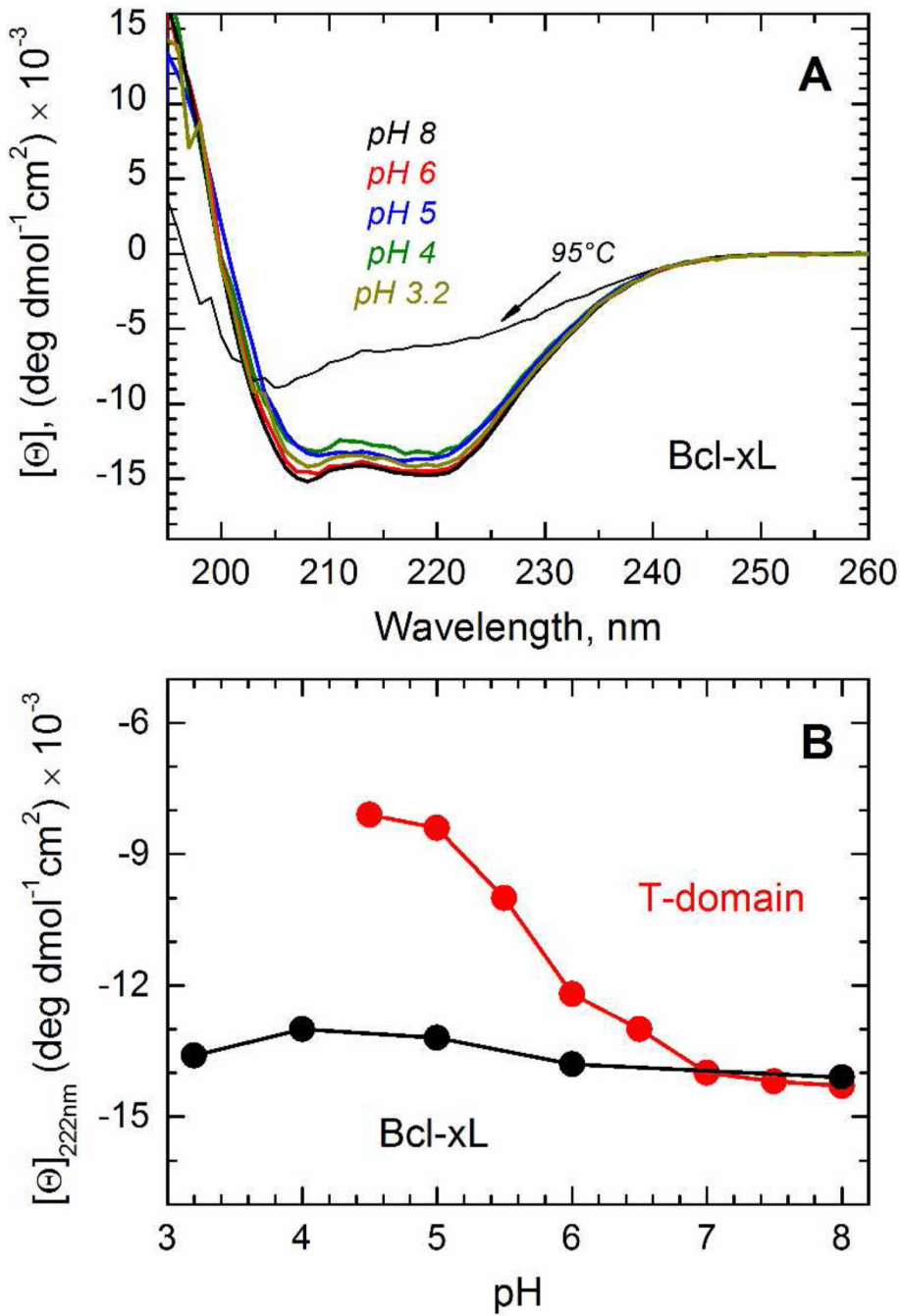
46. Chenal A, Savarin P, Nizard P, Guillain F, Gillet D, Forge V. Membrane protein insertion regulated by bringing electrostatic and hydrophobic interactions into play. A case study with the translocation domain of the diphtheria toxin. *J. Biol. Chem.* 2002; 277:43425–43432. [PubMed: 12193591]
47. Thuduppathy GR, Hill RB. Acid destabilization of the solution conformation of Bcl-xL does not drive its pH-dependent insertion into membranes. *Protein Sci.* 2006; 15:248–257. [PubMed: 16385002]
48. Fernandez MS, Fromherz P. Lipoid pH indicators as probes of electrical potential and polarity in micelles. *J. Phys. Chem.* 1977; 81:1755–1761.
49. Posokhov YO, Rodnin MV, Lu L, Ladokhin AS. Membrane insertion pathway of annexin B12: thermodynamic and kinetic characterization by fluorescence correlation spectroscopy and fluorescence quenching. *Biochemistry.* 2008; 47:5078–5087. [PubMed: 18407663]
50. Brooke JS, Cha JH, Eidels L. Diphtheria toxin:receptor interaction: association, dissociation, and effect of pH. *Biochem Biophys Res Commun.* 1998; 248:297–302. [PubMed: 9675130]

**FIGURE 1.**

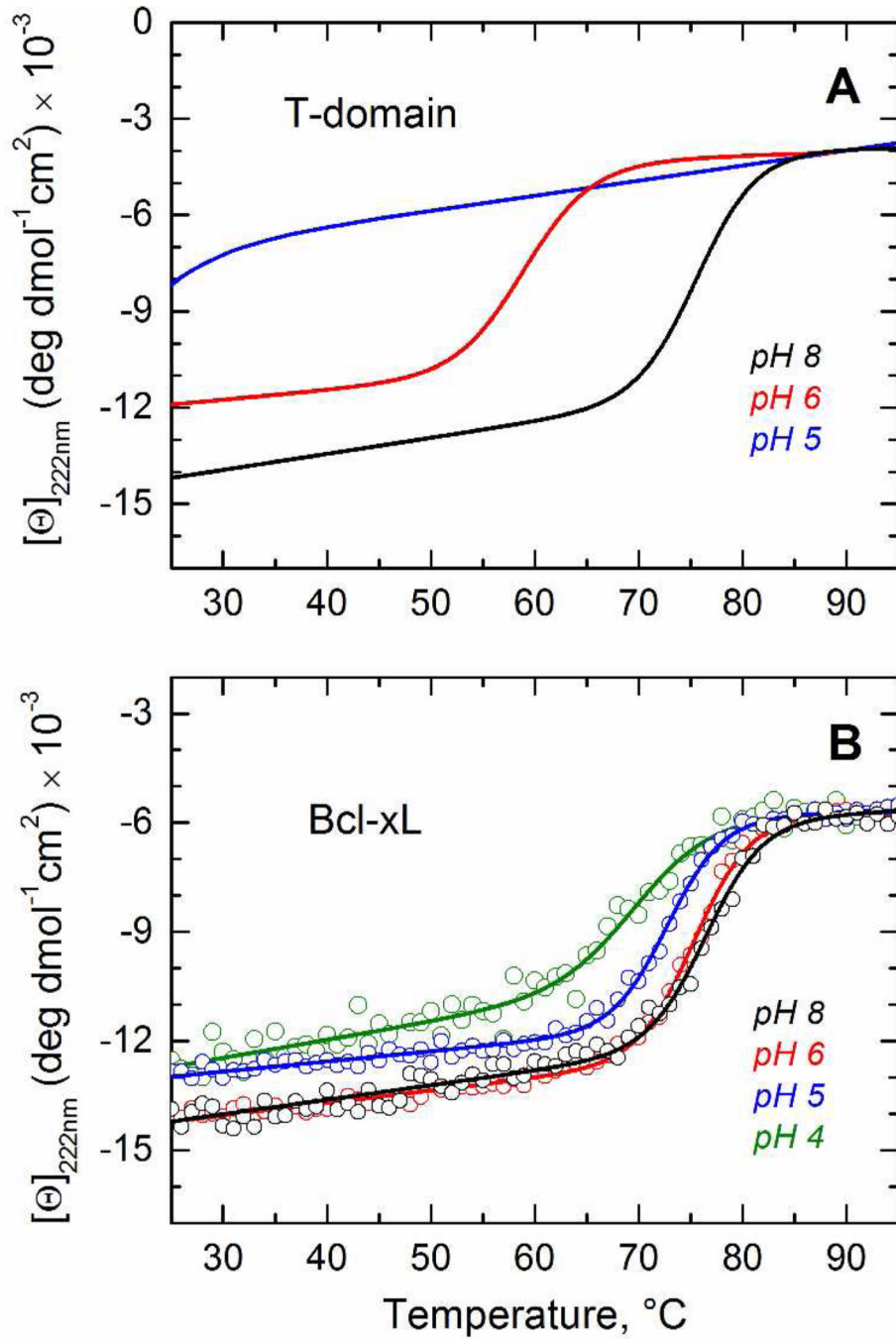
A) Crystal structure of the diphtheria toxin T-domain (PDB 1MDT) in solution at neutral pH (7). The central helices TH8–TH9 are highlighted in red, and the residues N235 and Q369, used for cysteine replacement for site-selective labeling in reference (13) are shown as CPK representations. B) NMR structure of Bcl-xL (PDB 1LXL) in solution (24), highlighting the helices α5 and α6 (red), and the residues G70, R102, S110 and N175, which were used for cysteine replacement for site-selective labeling in this study. The putative location of the truncated C-terminal TM helix is schematized with a dotted arrow.

**FIGURE 2.**

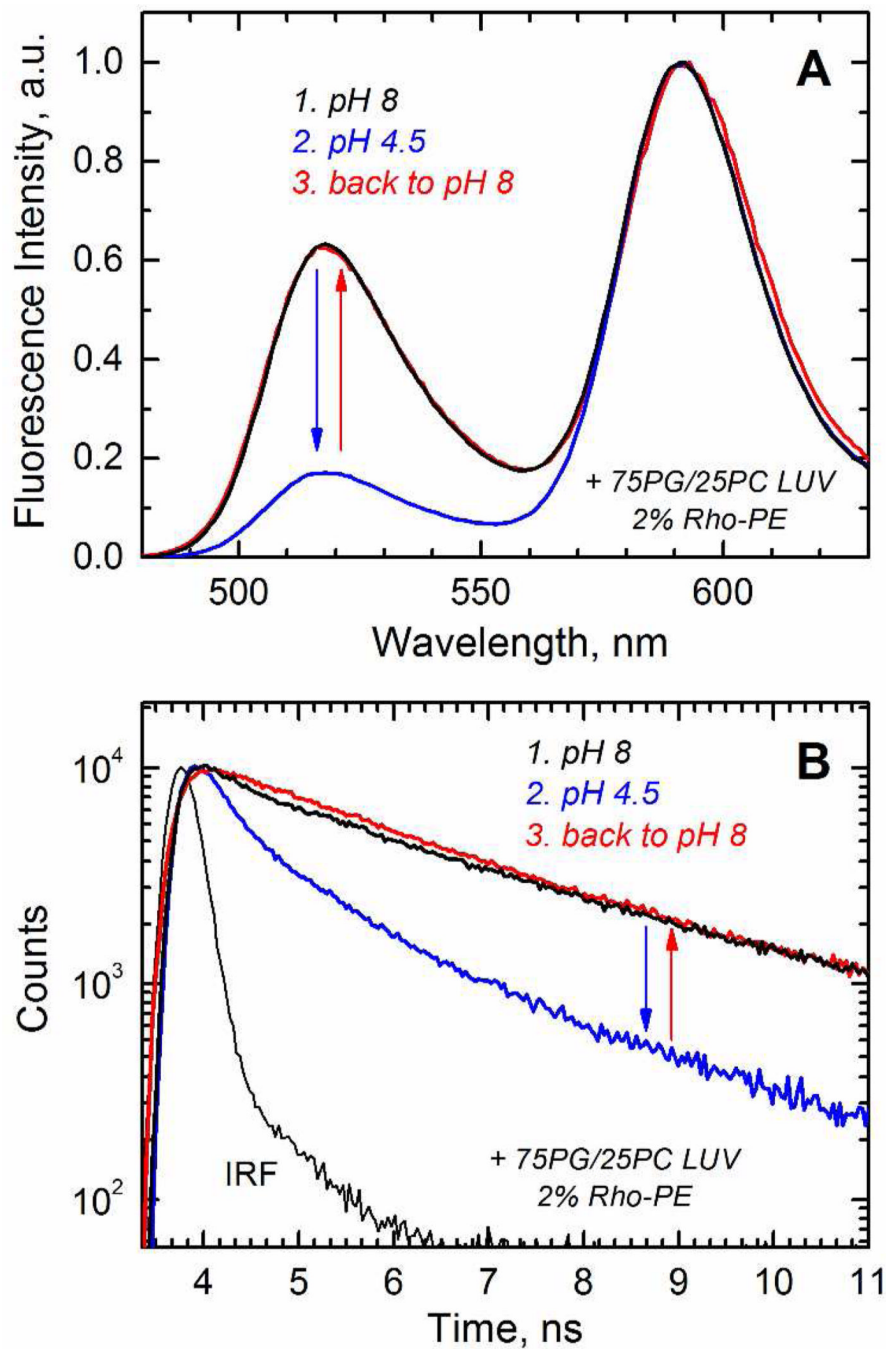
Schematic representation of the mode of attachment of the diphtheria toxin (A) and Bcl-xL (B) to their target membranes. The figure illustrates the equivalent attachment/anchor function of the TM helix and the R-domain for Bcl-xL and the diphtheria toxin, respectively. The membrane insertion of the T-domain and the N-terminal region of Bcl-xL occur regardless of the attachment to the membrane. The processes addressed in this study are shown as curved red arrows (see text for more).

**FIGURE 3.**

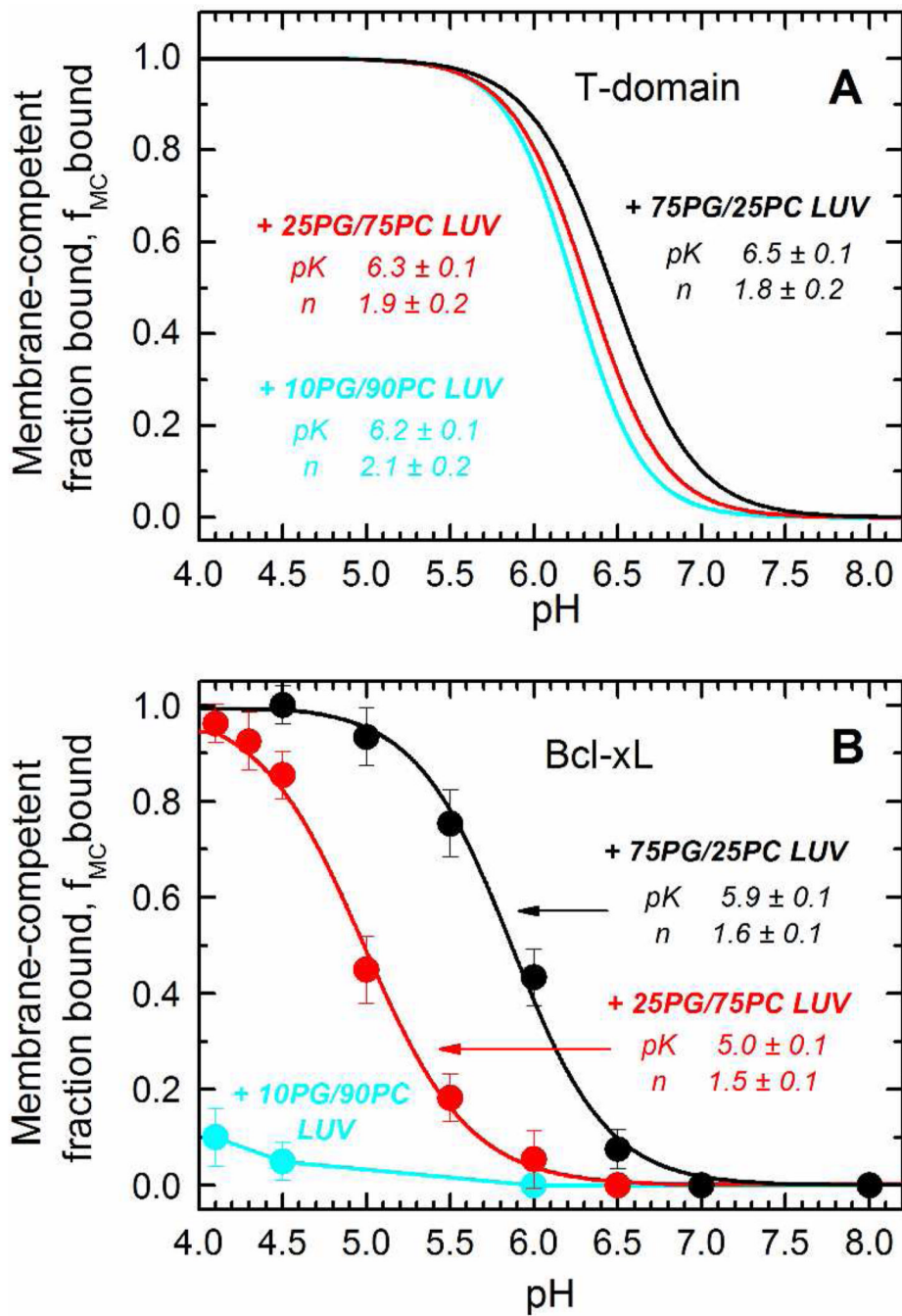
Comparison of pH-dependent variation in secondary structure and thermostability of Bcl-xL and the T-domain in solution. A) CD spectra of Bcl-xL in solution at pH 8 (black spectrum), 6 (red spectrum), 5 (blue spectrum), 4 (olive spectrum) and 3.2 (dark yellow spectrum) at 25°C. The CD spectrum at pH 8 and 95°C is shown for reference (dotted line). B) pH-dependent changes in molar ellipticity measured at 222 nm for T-domain (open symbols, data reproduced from (45) for visual comparison) and Bcl-xL (solid symbols).

**FIGURE 4.**

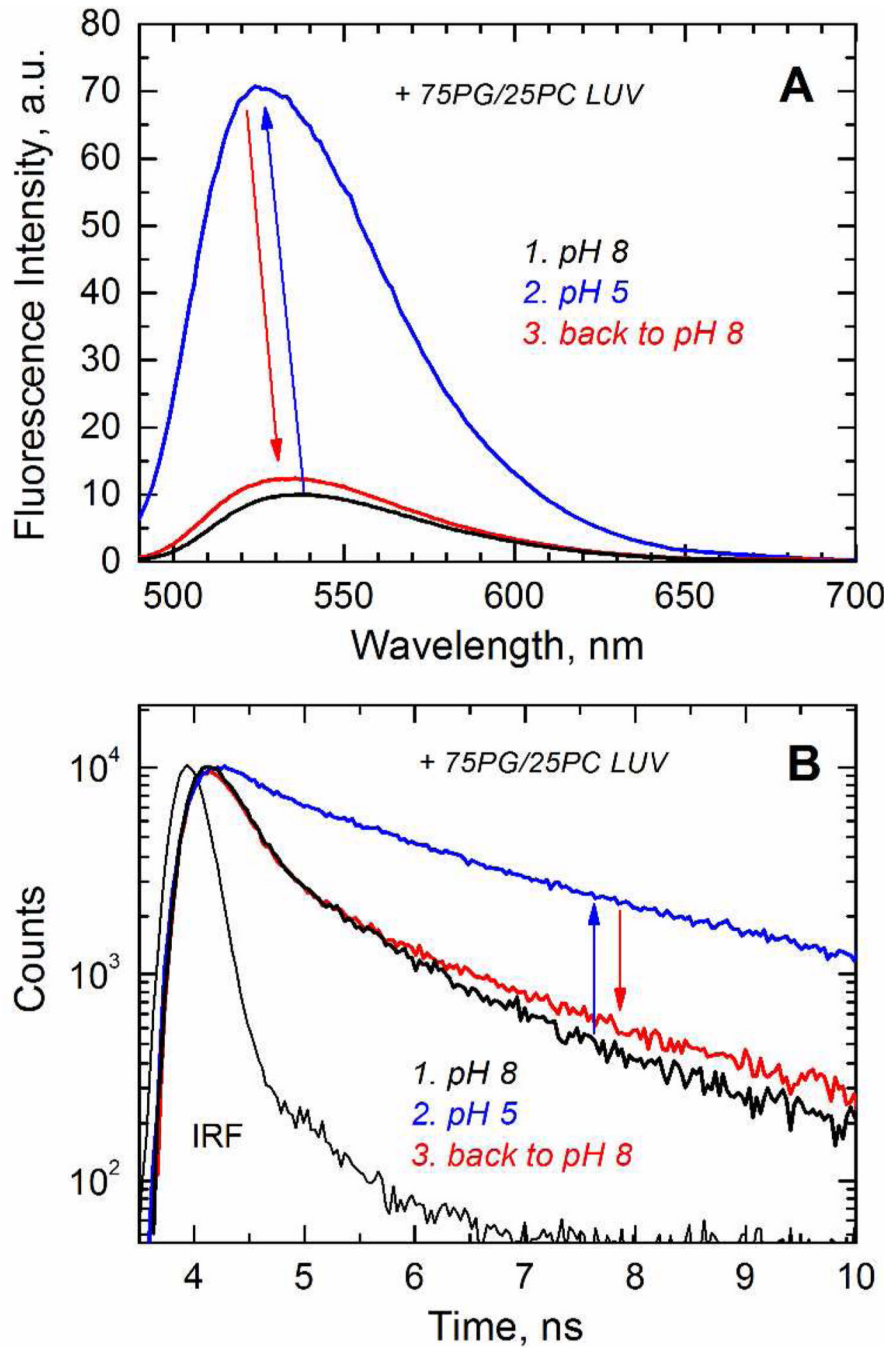
Comparison of pH-dependent variation in thermostability of Bcl-xL and the T-domain in solution. (Corresponding thermodynamic parameters are summarized in Table 1). A) Fitting curves of the previously published data (17) on thermal unfolding of the T-domain in solution at pH 8 and 6 are shown for reference. At pH 5 no cooperative melting transition can be detected. B) Thermal unfolding of Bcl-xL at pH 8 (black), pH 6 (red), pH 5 (blue) and pH 4 (olive). The figure illustrates the small effect of acidification on the secondary structure of Bcl-xL, contrasting with the dramatic loss of stability of the T-domain.

**FIGURE 5.**

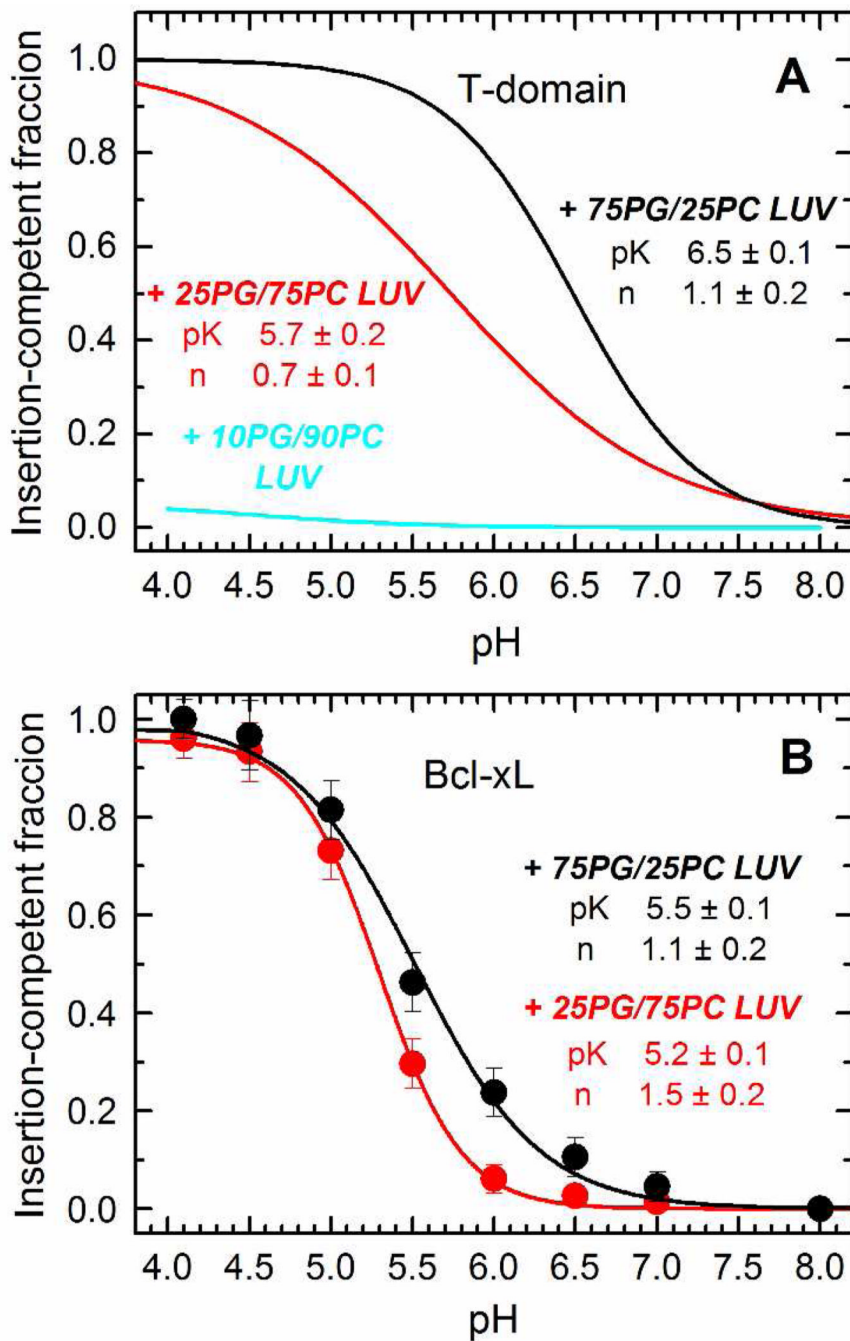
Reversibility of pH-dependent membrane association of Bcl-xL examined by the FRET measurements between donor-labeled protein and acceptor-labeled LUV. A) Emission spectra of the donor at pH 8 (step 1, black spectrum) and 4.5 (step 2, blue spectrum) in the presence of the acceptor. The loss of intensity is recovered upon addition of NaOH to return to pH 8 (step 3, red spectrum). B) Fluorescence decay of the donor at pH 8 (step 1, black trace) and 4.5 (step 2, blue trace) in the presence of the acceptor. The shortening of the decay is reversed upon return to pH 8 (step 3, red trace). The data indicate that the pH-triggered binding of Bcl-xL to the membrane is a reversible process.

**FIGURE 6.**

Comparison of pH-dependent binding of Bcl-xL and the T-domain to LUV composed of different mixtures of POPC and POPG. A) The binding of the T-domain to the membrane interface does not depend on the mole fraction of POPG, as the three lipid compositions result in almost identical titration curves (only fitting curves taken from reference (13) are shown). B) The titration curves of Bcl-xL shift to a lower pH when the mole fraction of POPG decreases from 75% (black) to 25% (red), with no detectable binding at 10% of POPG (cyan). The pK and n (Hill coefficient) were obtained by fitting the data to a two-state model as described in methods.

**FIGURE 7.**

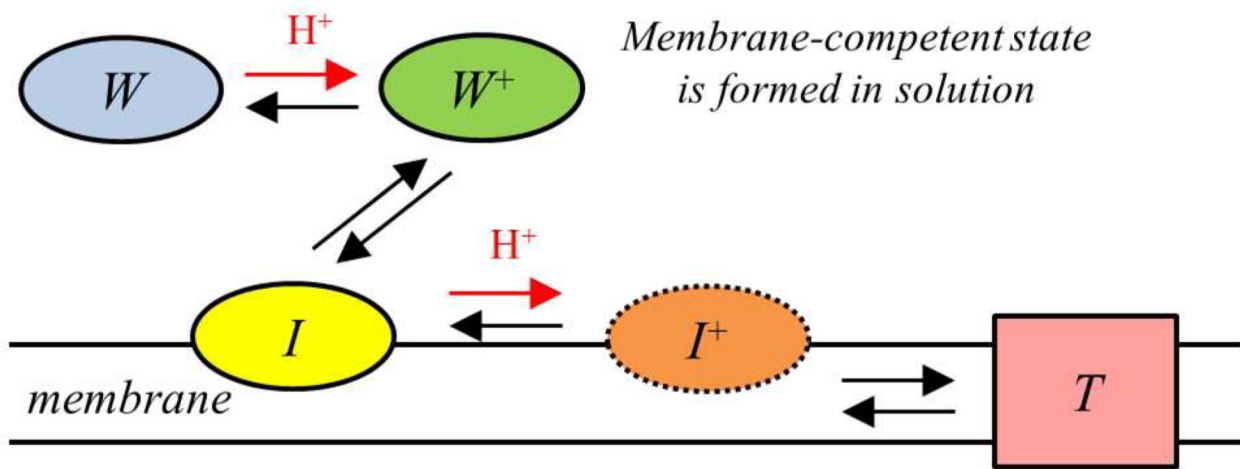
Reversibility of pH-dependent membrane insertion of Bcl-xL examined by a fluorescence assay based on the spectroscopic responses of the environment-sensitive probe NBD attached to the residue N175C in the middle of helix α 6. A) Emission spectra in the presence of LUV at pH 8 (step 1, black spectrum) and 5 (step 2, blue spectrum). There is a gain in intensity and a blue shift at acidic pH in the presence of LUV, and a recovery of spectral features upon return to pH 8 (step 3, red spectrum). B) Fluorescence decay of the same samples illustrating the broadening of the decay at acidic pH in the presence of LUV.

**FIGURE 8.**

Comparison of pH-dependent membrane insertion of the hydrophobic helical hairpins of the T-domain and Bcl-xL. A) The membrane insertion of the T-domain into LUV, determined as a function of the pH, strongly depends on the mole fraction of POPG in the LUV (only fitting curves from reference (13) are shown). B) The membrane insertion of Bcl-xL, studied as a function of the pH by following the changes in emission intensity at 525 nm, does not strongly depend on the POPG content of LUV (data in 90PC/10PG is omitted since there is no initial binding of the protein to LUV with this lipid composition). The data was fitted to a two-state model as described in methods.

pH-TRIGGERED MEMBRANE INSERTION

A *Diphtheria toxin T-domain*



B *Bcl-xL*

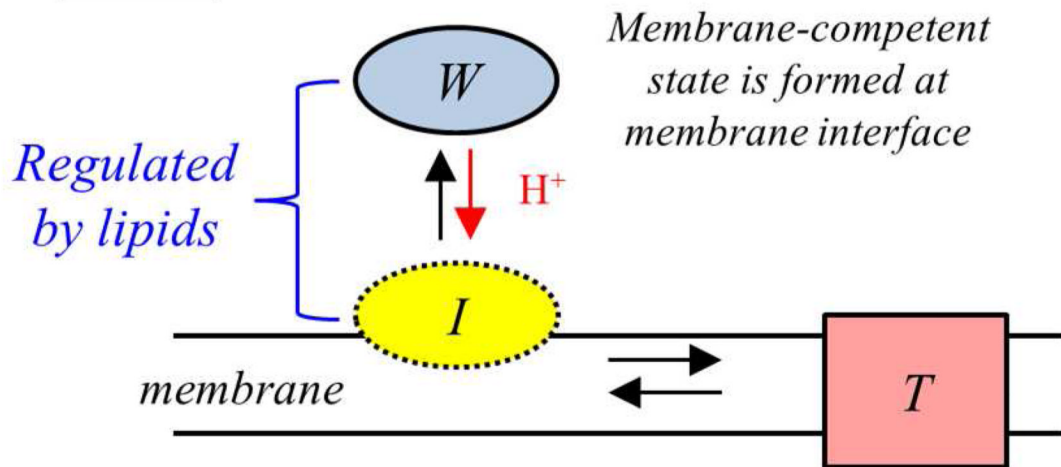


FIGURE 9.

Schematic representations of the pH-triggered membrane insertion pathways of the diphtheria toxin T-domain (A) and apoptotic regulator Bcl-xL (B). Each starts with a similarly folded soluble W-state (Fig. 1) and ends with membrane-inserted T-state, in which two central hydrophobic helices, TH8–TH9 of the T-domain and α 5– α 6 of the Bcl-xL, adopt a transmembrane conformation. The pathway connecting the two states, however, is very different in the two proteins. T-domain goes through a set of intermediate states and undergoes several protonation transitions, both in solution and on membrane interface, characterized by staggered pH-dependencies (13). Unlike the T-domain, Bcl-xL is not destabilized by acidic pH in solution, and protonation resulting in the formation of its

membrane-competent form occurs on membrane interface where it can be regulated by lipid composition. The interfacial intermediate state for Bcl-xL appears to be transient (as indicated by dotted border line of I-state on the scheme) with insertion closely following initial association with membrane interface (see Figs. 6 and 8, and text for details).

Table 1

Thermodynamic parameters for the thermal unfolding of the T-domain and Bcl-xL in solution at the indicated pH.

pH	T-domain*		Bcl-xL	
	Tm, °C	ΔH°, Kcal/mole	Tm, °C	ΔH°, Kcal/mole
8	75 ± 1	95 ± 7	77 ± 1	87 ± 6
6	59 ± 1	78 ± 6	76 ± 1	88 ± 4
5	No cooperative transition		73 ± 1	89 ± 4
4	No cooperative transition		70 ± 1	62 ± 8

* The parameters for the T-domain were previously published in reference (17).